Palaeogeography, Palaeoclimatology, Palaeoecology 655 (2024) 112505

Contents lists available at ScienceDirect

Palaeogeography, Palaeoclimatology, Palaeoecology

journal homepage: www.elsevier.com/locate/palaeo

Carbonate $\delta^{13}C$ chemostratigraphy of the Hunjiang Group in North China and a tentative stratigraphic framework for the Meso-Neoproterozoic transition

Junyao Kang [a,b], Qing Tang [c], Benjamin C. Gill [a,b], Rachel Reid [a,b], Wentao Zheng [d], Shuhai Xiao [a,b,*]

[a] *Department of Geosciences, Virginia Tech, Blacksburg, VA, USA*
[b] *Global Change Center, Virginia Tech, Blacksburg, VA, USA*
[c] *State Key Laboratory for Mineral Deposits Research, School of Earth Sciences and Engineering, and Frontiers Science Center for Critical Earth Material Cycling, Nanjing University, Nanjing, China*
[d] *Department of Earth Science, University of California, Santa Barbara, CA, USA*

ARTICLE INFO

Editor: Dr. Bing Shen

Keywords:
Meso-Neoproterozoic transition
Chemostratigraphic correlation
Carbon isotope
North China Craton
São Francisco Craton
Congo Craton

ABSTRACT

A robust stratigraphic framework for the Meso-Neoproterozoic transition is necessary for a better understanding of evolutionary and environmental changes during this critical geological time interval. Given the limited availability of radiometric and biostratigraphic data from late Mesoproterozoic to early Neoproterozoic strata, chemostratigraphic correlations have been used to build this framework. To contribute to Proterozoic chemostratigraphy, here we report new carbonate carbon isotope data from the Hunjiang Group in the Baishan area of Jilin Province in North China. The carbon isotope data (average 3.00 ‰ ± 1.15 ‰, 1 SD), together with existing detrital zircon constraints and microfossils, confirm a late Mesoproterozoic to early Neoproterozoic age of the Hunjiang Group. Using the dynamic time warping algorithm, we then constructed a global chemostratigraphic framework for the Meso-Neoproterozoic transition based on $\delta^{13}C_{carb}$ data from the North China, São Francisco, and Congo cratons. This exercise confirms the generally narrow range of $\delta^{13}C_{carb}$ fluctuations in the late Mesoproterozoic but also substantiates a negative $\delta^{13}C_{carb}$ excursion of notable magnitude (~9 ‰) and of potential global extent at ca. 1 Ga. This negative excursion, known as the Majiatun excursion, likely marks the Meso-Neoproterozoic transition and the onset of the dynamic carbon cycle in the Neoproterozoic Era.

1. Introduction

The Earth experienced critical biological and environmental changes at the Meso-Neoproterozoic transition, including important evolutionary innovations in early eukaryotes (Xiao and Tang, 2018), the rise of eukaryotes to ecological dominance (Brocks et al., 2017; Zumberge et al., 2020; Brocks et al., 2023), changes in macronutrient supply (Reinhard et al., 2017; Kang et al., 2023), and a transition from euxinic to ferruginous mid-depth oceans (Guilbaud et al., 2015). To understand these global changes and their underlying mechanisms, a robust temporal framework for this critical interval is imperative. However, the dearth of radiometric dates and index fossils from late Mesoproterozoic to early Neoproterozoic strata has hindered the application of chrono- and biostratigraphic correlations. Although several taxa have been proposed as potential index fossils, including *Cerebrosphaera* (Cornet et al., 2019) and *Trachyhystrichosphaera aimika* (Pang et al., 2020), their applicability is limited because they are rarely preserved in carbonate rocks, which constitute a significant portion of the late Mesoproterozoic to early Neoproterozoic sedimentary record. Conversely, carbonate carbon isotope ($\delta^{13}C_{carb}$) chemostratigraphy has long been validated as a useful tool for stratigraphic correlation of Precambrian carbonate rocks (Knoll and Walter, 1992; Halverson et al., 2005). However, as carbonate carbon isotope compositions can be influenced by local biological, sedimentary, and diagenetic processes (Higgins et al., 2018; Geyman and Maloof, 2019; Xiao et al., 2020; Geyman and Maloof, 2021; Trower et al., 2024), a comprehensive assessment of global carbon isotope signals requires chemostratigraphic data from multiple localities worldwide to provide a reliable basis for building a solid correlative

* Corresponding author at: Department of Geosciences, Virginia Tech, Blacksburg, VA, USA.
E-mail address: xiao@vt.edu (S. Xiao).

https://doi.org/10.1016/j.palaeo.2024.112505
Received 30 July 2024; Received in revised form 11 September 2024; Accepted 11 September 2024
Available online 13 September 2024

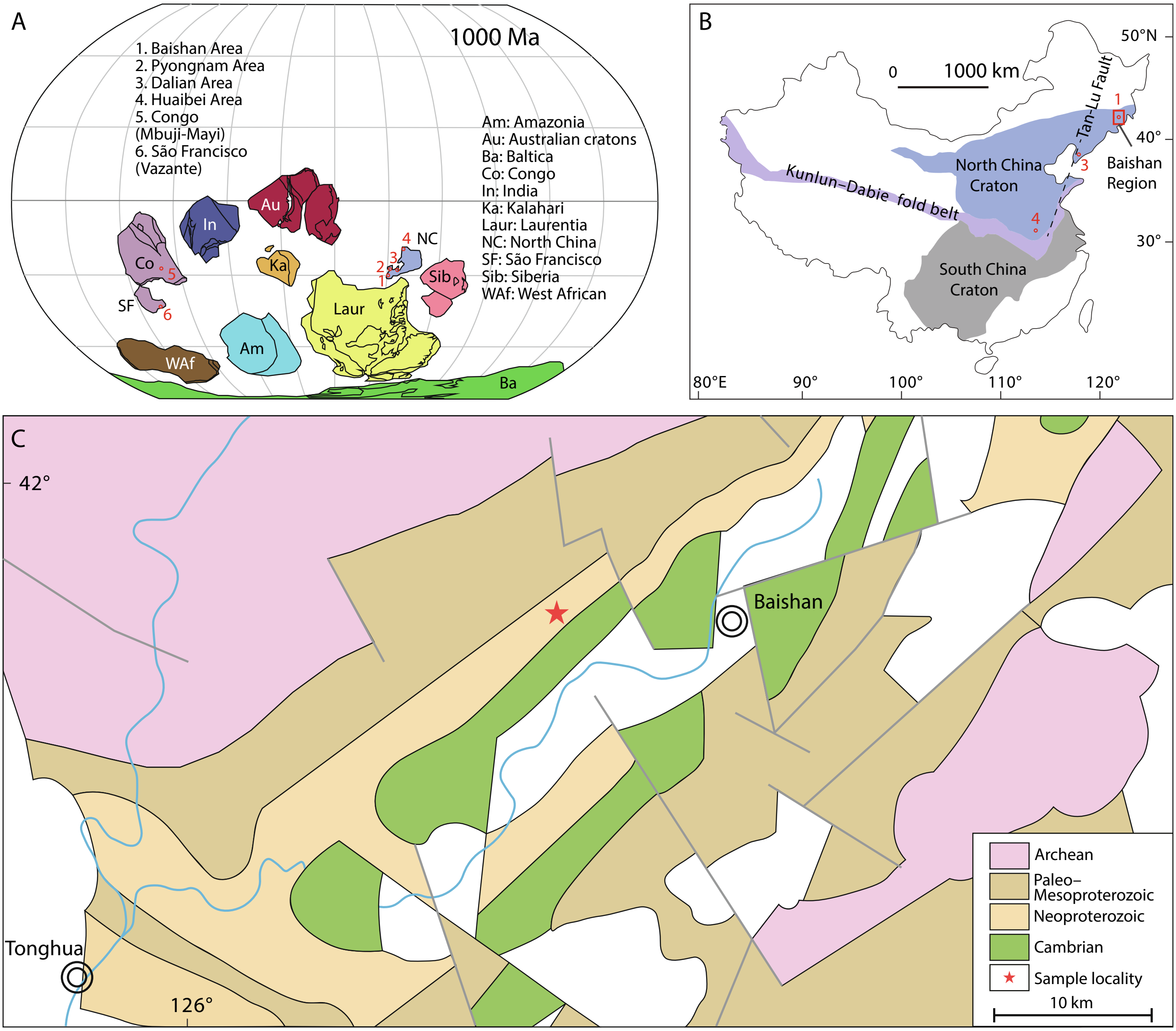

Fig. 1. Geological maps. (A) Paleogeographic reconstruction of the Rodinia supercontinent at ~1.0 Ga. Modified from Evans (2021). Locations of late Mesoproterozoic to early Neoproterozoic sections mentioned in this paper are marked as 1–6. (B) Simplified geological map of China showing the location of the Baishan region (red rectangle) in the North China Craton. Localities of late Mesoproterozoic to early Neoproterozoic sections are marked as 1 (Baishan), 3 (Dalian), and 4 (Huaibei). (C) Geological map of the Baishan region showing the sample location of the Hunjiang Group (red star). Modified from Zheng et al. (2023). (For interpretation of the references to colour in this figure legend, the reader is referred to the web version of this article.)

framework. In addition, conventional chemostratigraphic frameworks rely on visual interpretive correlations (Halverson et al., 2005), which may introduce subjectivity and potential bias. To mitigate these issues, the application of a dynamic time warping algorithm on carbon isotope chemostratigraphic correlations can be used to achieve stratigraphic correlations with statistical significance and reproducibility (Hay et al., 2019).

Late Mesoproterozoic to early Neoproterozoic strata exposed along the southeastern margin of the North China Craton (NCC) are crucial for illuminating the global picture of the Meso-Neoproterozoic transition, thanks to their minimal degree of metamorphic alteration, extensive stratigraphic coverage, and exceptional preservation of both macro- and microfossils (Yin, 1985; Dong et al., 2008; Xiao et al., 2014; Tang et al., 2015; Tang et al., 2020; Li et al., 2023). Carbonate carbon isotope data have been previously reported from late Mesoproterozoic to early Neoproterozoic sequences in several localities of NCC, including the Huaibei Group on the southern margin (Xiao et al., 2014), and the Wuxingshan (= Wuhangshan) and Jinxian groups and Sangwon Supergroup on the eastern margin (Park et al., 2016; Zhang et al., 2021). These data are important in establishing a comprehensive stratigraphic framework for the Meso-Neoproterozoic transition. Conversely, while the late Mesoproterozoic to early Neoproterozoic sequences (e.g., the Hunjiang Group) in the northeastern part of North China are impressive due to their significant thickness of carbonates and well-preserved microfossils in siliciclastics (Yin, 1987; Gao et al., 1995; Qiao et al., 1995; Zheng et al., 2023), there is a scarcity of chemostratigraphic data in this region, resulting in incomplete coverage of chemostratigraphic sequences in the NCC.

To address the knowledge gap of Meso-Neoproterozoic chemostratigraphy in the northeastern part of North China, in this study we obtained new $\delta^{13}C_{carb}$ data from the Hunjiang Group in the Baishan area of southern Jilin Province. After integrating the Baishan data with

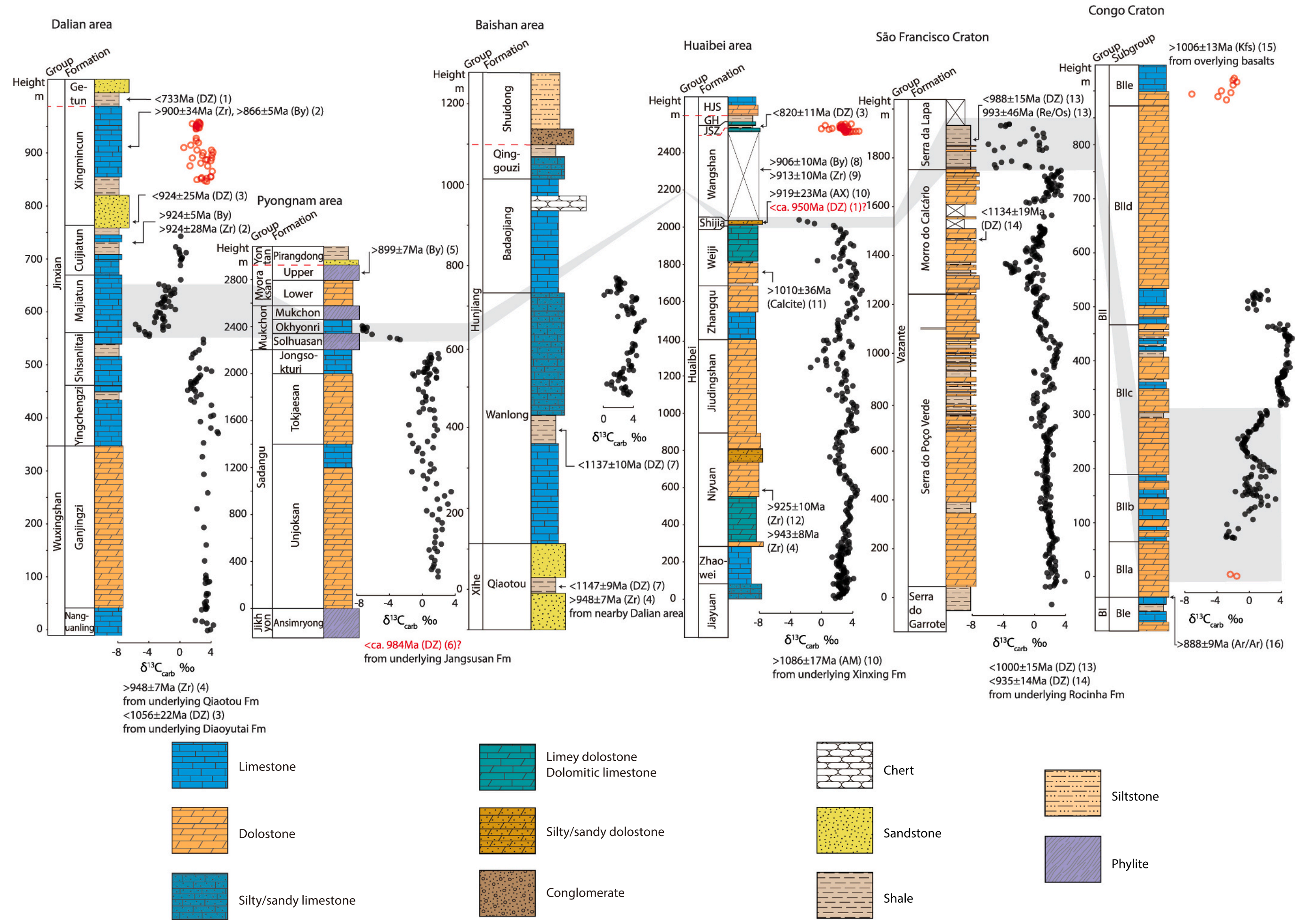

Fig. 2. Lithostratigraphic columns, chronostratigraphic constraints, and $\delta^{13}C_{carb}$ profiles of late Mesoproterozoic to early Neoproterozoic carbonate sequences from the North China, São Francisco, and Congo cratons. The chemostratigraphic data, from left to right, are from Zhang et al. (2021), Park et al. (2016), this study, Xiao et al. (2014), Alvarenga et al. (2019), and Delpomdor and Préat (2013). The gray band marks the ca. 1.0 Ga Majiatun negative $\delta^{13}C_{carb}$ excursion in the NCC and its likely correlatives in the São Francisco and Congo cratons (see details in the discussion). $\delta^{13}C_{carb}$ values marked as red open circles are not included in the DTW analysis since they are separated from the rest of the strata within the sequence by major depositional gaps. AM–authigenic monazite; AX–authigenic xenotime; By–baddeleyite; DZ–detrital zircon; Kfs–K-feldspar; Zr–magmatic zircon. Two age constraints from the Shijia Formation in the Huaibei area and the Jangsusan Formation in the Pyongnam area are marked with a question mark because they represent the youngest detrital zircon ages each based on only two zircon grains (see main text for discussion). References for radiometric ages: (1) He et al. (2017); (2) Zhang et al. (2016); (3) Yang et al. (2012); (4) Zhao et al. (2020); (5) Peng et al. (2011); (6) Hu et al. (2012); (7) Wen et al. (2020); (8) Su et al. (2021); (9) Zhu et al. (2019); (10) Zhang et al. (2022); (11) Lan et al. (2022); (12) Fu et al. (2015); (13) Azmy et al. (2008); (14) Rodrigues et al. (2012); (15) François et al. (2023); (16) Delpomdor et al. (2013b). $\delta^{13}C_{carb}$ data are included in Data files S1 and S2. (For interpretation of the references to colour in this figure legend, the reader is referred to the web version of this article.)

existing $\delta^{13}C_{carb}$ data and radiometric dates from multiple areas in the NCC, we used the dynamic time warping algorithm (Hay et al., 2019) to build a relatively complete $\delta^{13}C$ record for the Meso-Neoproterozoic transition in the NCC. Finally, using the same algorithm, we correlated the NCC record with previously published $\delta^{13}C$ data and geochronometric constraints from the São Francisco and Congo cratons to attempt a global chemostratigraphic correlative framework for the late Mesoproterozoic to early Neoproterozoic Era (Fig. 1).

2. Stratigraphic settings and sample localities

The NCC, which was stabilized around 1.9 Ga (Kusky and Li, 2003; Zhao et al., 2003; Zhai et al., 2015), is one of the most extensively examined cratons globally. Multiple Proterozoic sedimentary basins developed on the NCC from ca. 1.9 Ga to ca. 0.9 Ga (Zhai et al., 2015). At ca. 1.1 Ga, siliciclastic and carbonate sediments started to accumulate in the Xuhuai rift system along the southeastern margin of the NCC (Meng et al., 2011; Su et al., 2020; Sun et al., 2020). The Xuhuai rift system was later offset by the Triassic-Jurassic strike-slip Tan-Lu fault (Xu et al., 1987; Zhu et al., 2005), and the late Mesoproterozoic to early Neoproterozoic sedimentary strata are now distributed in the Baishan, Pyongnam, Dalian, Huaibei, Huainan, and Jiaolai areas (Fig. 1A–B).

Available radiometric ages indicate that Meso-Neoproterozoic successions in the NCC discussed in this paper are ~1000 Ma in age or slightly older (Fig. 2). In the Huaibei area, for example, in-situ carbonate U-Pb dating of the Weiji Formation of the Huaibei Group gave ages of 1036 ± 45 Ma and 1010 ± 36 Ma (Lan et al., 2022), whereas the uppermost sediments of the group are attributed to the Tonian period (Yang et al., 2012; Zhang et al., 2016; He et al., 2017) (Fig. 2). Ages of magmatic intrusions in Meso-Neoproterozoic successions in the NCC typically fall within the range of 1000 and 900 Ma (Fig. 2), providing minimum constraints on depositional age. The youngest detrital zircons from these successions are mostly >1000 Ma, although those from the Xingmincun Formation in the Dalian (Yang et al., 2012), the Shijia Formation in the Huaibei area (He et al., 2017), and the Jangsusan Formation in the Pyongnam area (Hu et al., 2012) can be younger, in the range of 900–1000 Ma, suggesting an early Tonian age (Fig. 2). However, the Xingmincun Formation is at the very top of the Meso-

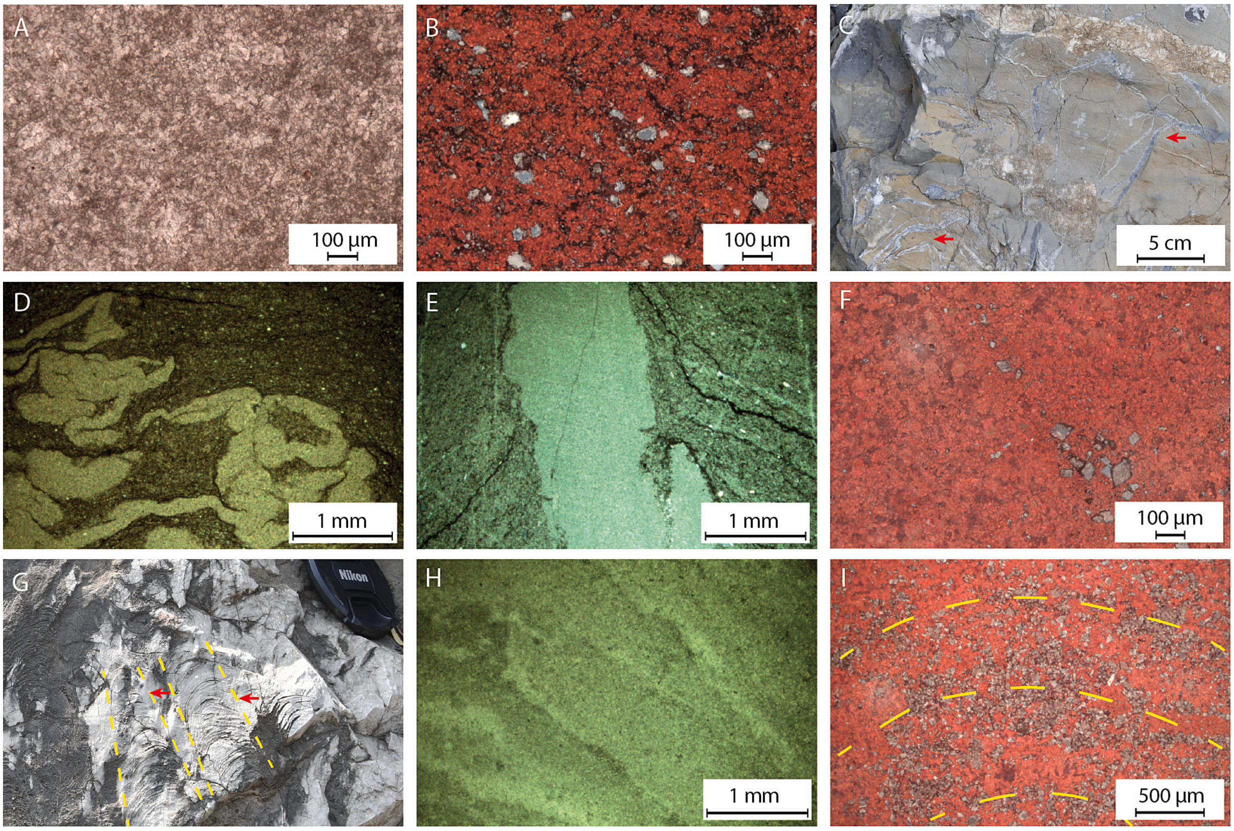

Fig. 3. Field and petrographic photographs of the Wanlong and Badaojiang formations in the Baishan region. (A) Transmitted light photomicrograph of Alizarin Red S or ARS-stained limey dolostone of the uppermost Wanlong Formation. (B) Transmitted light photomicrograph of ARS-stained silty limestone of the upper Wanlong Formation, under cross-polarized light. (C) Molar tooth structures (red arrows) from the Wanlong Formation in outcrop view. (D–E) Transmitted light photomicrograph of molar tooth structures under cross-polarized light. (F) Transmitted light photomicrograph of ARS-stained limestone of the Badaojiang Formation. Unstained crystals are dolomite rhombs. (G–I) Stromatolites in the Badaojiang Formation. (G) Field photograph of stromatolite (red arrows). Yellow dashed lines denote boundaries between columnar stromatolites and matrix sediment. (H) Transmitted light photomicrograph at lower magnification to better illustrate laminae in stromatolitic limestone. (I) Transmitted light photomicrograph of ARS-stained stromatolitic limestone. Yellow dashed lines denote stromatolitic laminae that are better discernable on hand samples. All transmitted light photomicrographs were taken under plane-polarized light except otherwise noted. (For interpretation of the references to colour in this figure legend, the reader is referred to the web version of this article.)

Neoproterozoic succession, and the Shijia and Jangsusan ages are based on only two zircon grains (Hu et al., 2012; He et al., 2017), raising caution about these latter age constraints because of possible lead loss.

The sampled Baishan section is located in southern Jilin Province. Here, a sedimentary sequence of late Mesoproterozoic to early Neoproterozoic age sits unconformably above the metamorphic basement of the Mesoproterozoic Laoling Group and below the phosphatic conglomerate of the early Cambrian Shuidong Formation (Bureau of Geology and Mineral Resources of Jilin Province, 1988) (Figs. 1C and 2). The sequence consists of, in ascending order, the Baifangzi Formation, the Xihe Group, and the Hunjiang Group. The Xihe Group, including the Diaoyutai, Nanfen, and Qiaotou formations, is dominated by quartz sandstone, silty shale, and shale. The Hunjiang Group, which conformably overlies the Xihe Group and is divided into the Wanlong, Badaojiang, and Qinggouzi formations in ascending order, is dominated by limestone, silty limestone, dolomitic limestone, and black shale. Microfossils characteristic of late Mesoproterozoic to early Neoproterozoic age, including *Trachyhystrichosphaera aimika* and *Proterocladus antiquus*, have been reported from the Qinggouzi Formation (Zheng et al., 2023). In this study, we focused on carbonate strata of the upper Wanlong Formation and lower Badaojiang Formation, which outcrop in the Baishan section. In the Wanlong Formation, the sampled interval transitions from silty/sandy to dolomitic limestone (carbonate mudstones) (Figs. 2 and 3A–E). Molar tooth structures, which are composed of homogenous microsparitic calcite and show evidence of pre-compaction cementation, are pervasive in the silty carbonate mudstones (Fig. 3C–E). In the Badaojiang Formation, the sampled interval consists of lime mudstone and stromatolitic boundstones (Figs. 2 and 3F–I). Stromatolites in the Badaojiang Formation consist of dark- and light-colored laminae, with the former typically composed of rhombic dolomite crystals (Fig. 3G–H).

The depositional ages of the Xihe and the Hunjiang groups are loosely constrained (Fig. 2). Detrital zircon data place a maximum depositional age of 1147.3 ± 9.08 Ma on the Qiaotou Formation, and 1137.4 ± 9.84 Ma on the Wanlong Formation (Wen et al., 2020). Additionally, the youngest detrital zircons from the Diaoyutai Formation in the Dalian area to the south yield an age of 1056 ± 22 Ma (Yang et al., 2012), and a diabase sill intruding the Qiaotou Formation of the Xihe Group that underlies the Wuxingshan Group in the Dalian area has been dated at 947.8 ± 7.4 Ma (Zhao et al., 2020). Thus, the sampled interval of this study can be broadly constrained between late Mesoproterozoic to early Neoproterozoic based on available biostratigraphic and radiometric data.

3. Methods

In this study, 85 carbonate samples were collected from the Wanlong and Badaojiang formations of the Hunjinag Group at the Taipinghu Outcrop, Baishan, Jilin, China (41°54′24.24″N, 126°18′09.26″E) (Fig. 1C). Standard petrographic thin sections were made and examined on a Zeiss Axioscope A1 microscope with an Axiocam 512 digital camera, and an Olympus SZ16 microscope with a DP27 digital camera at

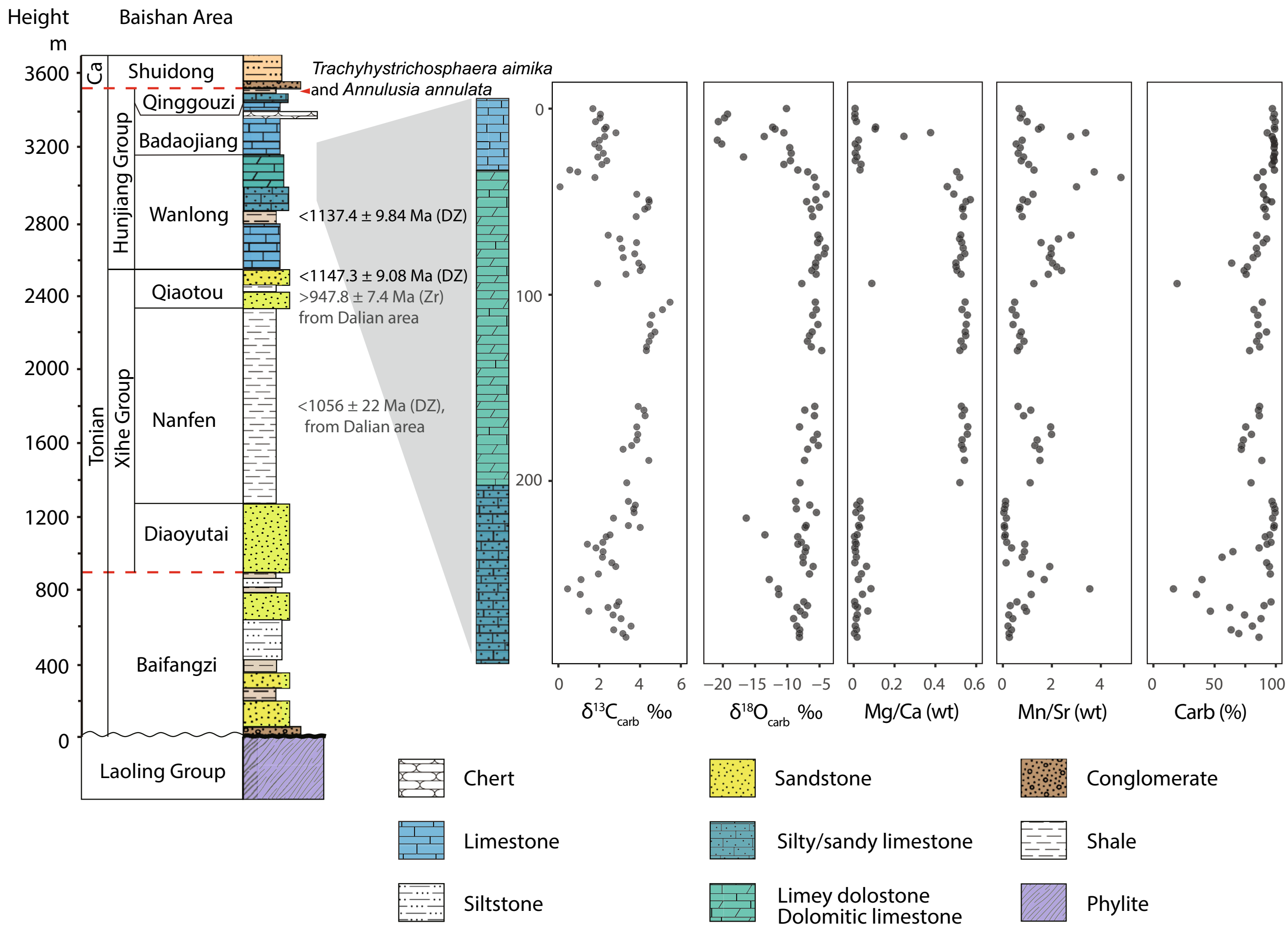

Fig. 4. Lithostratigraphic columns, chronostratigraphic constraints, and geochemical profiles ($\delta^{13}C_{carb}$, $\delta^{18}O_{carb}$, Mg/Ca, Mn/Sr, carbonate content) of the Hunjiang Group in the Baishan region. Radiometric dates (see text for references) and fossil occurrences are marked at their approximate stratigraphic horizons. Red dashed lines within the lithostratigraphic columns represent unconformities. Ca = Cambrian. $\delta^{13}C_{carb}$ data are included in Data file S1. (For interpretation of the references to colour in this figure legend, the reader is referred to the web version of this article.)

Virginia Tech. Guided by petrographic observations, powders for geochemical analyses were taken from freshly cut carbonate samples using a Dremel microdrill.

3.1. Geochemical Analysis

Carbonate $\delta^{13}C$ and $\delta^{18}O$ measurements were conducted at Virginia Tech on an Isoprime 100 Isotope Ratio Mass Spectrometer coupled to a MultiFlowGEO headspace analyzer. For each sample, 0.4–0.6 mg of powder was treated overnight with glacial phosphoric acid at 70 °C. The evolved CO_2 was then analyzed on the mass spectrometer. Sample carbon and oxygen isotope compositions were normalized to the Vienna Pee Dee belemnite (VPDB) scale. IAEA-CO-1 ($\delta^{13}C = 2.492 \pm 0.030$ ‰, $\delta^{18}O = -2.4 \pm 0.1$ ‰), IAEA-CO-9 ($\delta^{13}C = -47.321 \pm 0.030$ ‰, $\delta^{18}O = -15.6 \pm 0.2$ ‰), and NIST NBS-18 ($\delta^{13}C = -5.014 \pm 0.035$ ‰, $\delta^{18}O = -23.2 \pm 0.1$ ‰) were used as carbon and oxygen isotope standards. The precision of carbonate carbon isotope analysis was 0.14 ‰ (1 SD), based on repeated measurements of IAEA-CO-1 ($n = 8$), IAEA-CO-9 (n = 8), and NIST NBS-18 (n = 8). The precision of carbonate oxygen isotope analysis was 0.49 ‰ (1 SD), based on repeated measurements of IAEA-CO-1 (n = 8), IAEA-CO-9 (n = 8), and NIST NBS-18 (n = 8).

Elemental concentrations of Mg, Ca, Mn, and Sr were analyzed at Virginia Tech on an inductively coupled plasma mass spectrometer (ICP-MS). For each sample, approximately 0.1 g of powder was dissolved in glacial acetic acid. After complete digestion, samples were centrifuged, and the supernatant was separated. The supernatant was dried down and redissolved in 1 % acetic acid, which was then analyzed for major and trace element concentrations on a Thermo Electron iCAP-RQ ICP-MS per Standard Method 3125-B (American Public Health Association et al., 1998). The precision for Mg, Ca, Mn, and Sr concentrations is better than 5 %.

3.2. Dynamic Time Warping

Dynamic time warping (DTW) is a dynamic programming technique widely used to compare and align time-series datasets. In geosciences, DTW has been applied to the alignments of paleoclimate records (Lisiecki and Lisiecki, 2002; Hagen and Harper, 2023), secular paleomagnetic variations (Hagen et al., 2020), and carbon isotope chemostratigraphy (Hay et al., 2019; Hagen et al., 2024; Hagen and Creveling, 2024). In this study, the algorithm by Hay et al. (2019) was used to align chemostratigraphic data from the North China, São Francisco, and Congo cratons.

To align a candidate sequence (y_m) to a target sequence (x_n), an n × m cost matrix containing all feasible pairings between data points from these two sequences is constructed. The value of each element in the cost matrix is determined by calculating the squared difference between a data point in the target sequence and its corresponding data point in the candidate sequence. The goal is to find an optimal path that matches each index (m) from the candidate sequence to an index (n) in the target sequence while minimizing the sum of the cost matrix across all m (Hay et al., 2019). This algorithm employs two stratigraphically significant

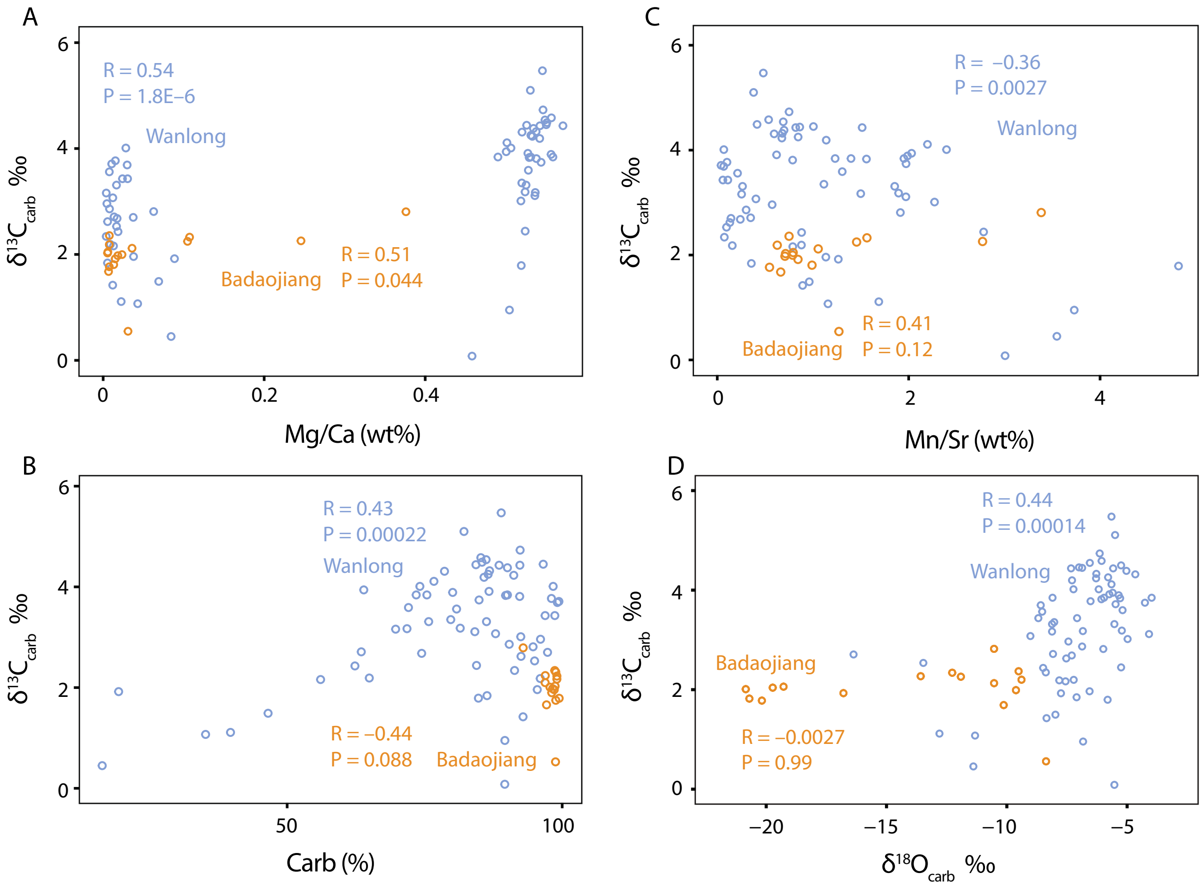

Fig. 5. Cross-plots of $\delta^{13}C_{carb}$ vs. Mg/Ca, Mn/Sr, carbonate content, and $\delta^{18}O_{carb}$. R and *p* values were calculated using Pearson correlation coefficient. Symbols are colour coded to differentiate data from the Wanlong and Badaojiang formations. All correlations are relatively weak. See text for discussion. Data are included in Data files S1.

parameters to determine the optimal alignment: the edge and g parameters. The edge parameter regulates the extent of overlap between the two sequences, with a higher edge value promoting a stronger degree of overlap (Sakoe and Chiba, 1978; Hay et al., 2019). The g parameter characterizes the similarity in sediment accumulation rates between the two sections during the shared depositional interval, where a value of g greater than one penalizes stretching and/or squeezing of the candidate sequence (Sakoe and Chiba, 1978; Hay et al., 2019). Once the two sequences are aligned, the cross-correlation at zero lag of the overlapped interval, which equals the Pearson correlation coefficient, is calculated when the overlap is >10 %. The statistical significance (*p*-value) of the correlation is then evaluated by the *t*-test statistic. In this study, alignments were calculated for all combinations of edge values ranging from 0.01 to 0.25 with increments of 0.01 and g values ranging from 0.98 to 1.01 with increments of 0.01. When comparing two sections, we explored two distinct scenarios. In each scenario, one section was designated as the target sequence while the other served as the candidate sequence. The alignment with the highest cross-correlation value, after considering geologic constraints (e.g., radiometric dates, depositional hiatuses, see sections 5.3 and 5.4 for details), was adapted to build the stratigraphic framework.

In this study, late Mesoproterozoic to early Neoproterozoic $\delta^{13}C_{carb}$ data from Dalian of Liaoning Province (Zhang et al., 2021), Pyongnam of North Korea (Park et al., 2016), Baishan of Jilin Province (this study), and Huaibei of Anhui and Jiangsu provinces (Xiao et al., 2014) were chosen for DTW analysis to construct a composite chemostratigraphic sequence for the NCC, which is then aligned with $\delta^{13}C_{carb}$ data from the São Francisco Craton (Alvarenga et al., 2019) and the Congo Craton (Delpomdor and Préat, 2013) using DTW to obtain a global chemostratigraphic sequence. To improve the accuracy of alignments, the uppermost parts of the Dalian, Huaibei, and Congo sequences (i.e., the Xingmincun, Jinshanzhai, Gouhou, BIIe, and BIIa formations/groups; see red open circles in Fig. 2), which are separated from the rest of the strata within the sequence by major depositional gaps, were removed before DTW analysis. Throughout the analysis, a sequential correlation approach was employed. Each new sequence is correlated with the aggregated sequence resulting from the previous correlation step (e.g., the Pyongnam and Dalian sections can be aligned and merged first, then the Huaibei section can be correlated with the newly aggregated dataset that combines the Pyongnam and Dalian data).

4. Results

Geochemical data tables are provided in the supplementary material. The $\delta^{13}C_{carb}$ values of the Wanlong and Badaojiang formations at the Baishan section are consistently positive and fall between 0 and 5 ‰ (average 3.0 ± 1.2 ‰, 1 SD; Figs. 2, 4 and 5). From the Wanlong to the Badaojiang Formation, the $\delta^{13}C_{carb}$ values show a small-scale increasing and then decreasing trend. The variation in $\delta^{13}C_{carb}$ is decoupled from that of $\delta^{18}O_{carb}$, which is mostly between −4 ‰ and − 8 ‰ in the Wanlong Formation and between −8 ‰ and − 21 ‰ in the Badaojiang Formation. For the Wanlong and Badaojiang formations, carbonate contents and Mg/Ca ratios are consistent with the carbonate mineralogy of the units. Mn/Sr ratios (average 1.1 ± 1.0, 1 SD) are relatively low throughout the measured section.

Late Mesoproterozoic to early Neoproterozoic $\delta^{13}C_{carb}$ chemostratigraphic records from North China, São Francisco, and Congo cratons (Fig. 2) were correlated using DTW. The alignment between the

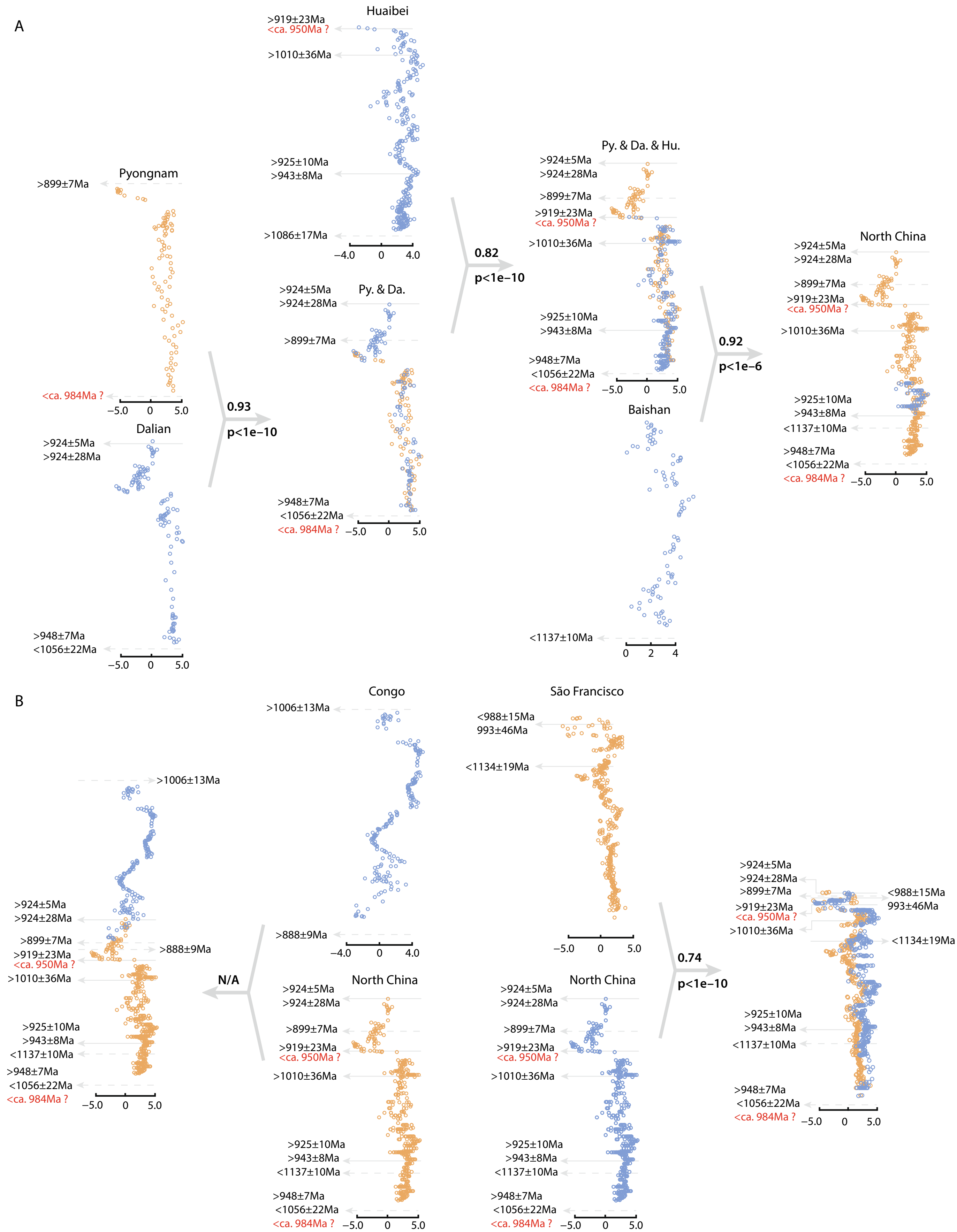

(caption on next page)

Fig. 6. Chemostratigraphic correlations among sections from NCC (A), and with sections from São Francisco and Congo cratons (B), using dynamic time warping (DTW). When comparing two sequences, the blue-colored sequence is the candidate sequence and the tan-colored sequence is the target sequence. After each sequential alignment, the data from the target and candidate sequences are combined, and the combined sequence serves as the target sequence for the next round of alignment. The numbers above and below the arrows are cross-correlation values and p values of the alignments, respectively. See Fig. 2. caption for sources of radiometric ages. Arrows with a thin solid line represent ages within the target strata. Arrows with a thin dashed line represent ages above or below the target strata. $\delta^{13}C_{carb}$ data are included in Data files S1 and S2. (For interpretation of the references to colour in this figure legend, the reader is referred to the web version of this article.)

Pyongnam and Dalian sequences yielded a maximum cross-correlation value of 0.93 (p < 1e–10, g = 0.98, edge = 0.08; Fig. 6A). Subsequently, the alignment between the Huaibei sequence and the newly merged dataset containing the Pyongnam and Dalian data produced a maximum cross-correlation value of 0.82 (p < 1e–10, g = 0.98, edge = 0.11; Fig. 6A). Next, the addition of the Baishan data yielded a maximum cross-correlation value of 0.92 (p < 1e–6, g = 0.98, edge = 0.04; Fig. 6A). Finally, for the correlation between the North China Craton and São Francisco Craton (the Vazante Group), an alignment with a cross-correlation value of 0.74 (p < 1e–10, g = 1.0, edge = 0.22, Fig. 6B) was selected (see discussion in section 5.4). For the alignment between the North China Craton and Congo Craton (the Mbuji-Mayi Supergroup), the cross-correlation value was not calculated because the overlap is less than 10 % (Fig. 6B).

5. Discussion

5.1. Evidence for primary marine signals

Based on the available petrographic, paleontological, and geochemical data, we argue that $\delta^{13}C_{carb}$ values from the Baishan sequence reflect primary oceanic signals. First, the sampled carbonates are mostly micritic limestones, with only minor dolomitization in some samples (Fig. 3B, F, and G). Additionally, molar tooth structures, which consist of homogenous calcite microspar thought to have precipitated during early diagenesis from porewater in direct connection with seawater (Kriscautzky et al., 2022), are abundant in the Wanlong Formation. The exceptional fossil preservation in the Qinggouzi Formation (Zheng et al., 2023), which overlies the Badaojiang Formation, also suggests low degrees of thermal maturity and diagenetic alteration. Second, although there is a weak correlation between $\delta^{13}C_{carb}$ values and Mg/Ca ratios (Fig. 5A–B), $\delta^{13}C_{carb}$ fluctuations, which can be driven by dolomitization (Bold et al., 2020), do not coincide with the lithological shift and the Mg/Ca change observed at the middle of the Wanlong Formation (Fig. 4). Hence, $\delta^{13}C_{carb}$ values are not primarily controlled by carbonate mineralogy. Instead, the higher $\delta^{13}C_{carb}$ values of dolomitic limestone in the upper Wanlong Formation and lower $\delta^{13}C_{carb}$ values of limestone in the Badaojiang Formation may reflect secular changes of oceanic signals. Third, as diagenesis tends to enrich Mn but deplete Sr (Brand and Veizer, 1980; Swart, 2015), the low Mn/Sr ratios (<2) of the Baishan samples suggest minimal diagenetic alterations (Kaufman and Knoll, 1995) (Fig. 4). This assessment is consistent with the weak correlation between $\delta^{13}C_{carb}$ values and Mn/Sr ratios (Fig. 5C). Fourth, although $\delta^{18}O_{carb}$ exhibits large variations, $\delta^{13}C_{carb}$ remains in a relatively narrow range, resulting in a rather weak correlation between $\delta^{13}C_{carb}$ and $\delta^{18}O_{carb}$ (Fig. 5D, R = 0.44 for Wanlong samples, $R = -0.0027$ for Badaojiang samples), and indicating that $\delta^{13}C_{carb}$ is better buffered against diagenetic alteration than is $\delta^{18}O_{carb}$ (Brand and Veizer, 1981; Lau and Hardisty, 2022). While additional diagenetic evaluation of published late Mesoproterozoic to early Neoproterozoic $\delta^{13}C_{carb}$ data from North China, São Francisco, and Congo cratons is beyond the scope of this paper, previous petrographic, paleontological, and geochemical (i.e., $\delta^{18}O_{carb}$, $^{87}Sr/^{86}Sr$, Mn/Sr, Fe/Sr, REE + Y) evidence suggests the preservation of primary oceanic signals (Delpomdor et al., 2013a; Xiao et al., 2014; Park et al., 2016; Alvarenga et al., 2019; Zhang et al., 2021).

5.2. Age constraints of the Baishan succession

The new chemostratigraphic data from the Baishan sequence, combined with existing geochronological and paleontological data, suggest a late Mesoproterozoic to early Neoproterozoic age of the Hunjiang Group. The late Mesoproterozoic to early Neoproterozoic $\delta^{13}C_{carb}$ record is characterized by consistently positive values with moderate variation (mostly between 0 ‰ and 5 ‰) (Xiao et al., 2014). Therefore, $\delta^{13}C_{carb}$ values (average 3.00 ± 1.15 ‰, 1 SD) recorded in the Wanlong and Badaojiang formations are consistent with a late Mesoproterozoic to early Neoproterozoic age (Fig. 4). This inference is also supported by detrital zircon data (1147.3 ± 9.08 Ma) from the underlying Qiaotou Formation (Wen et al., 2020) and the occurrence of *Trachyhystrichosphaera aimika* and *Proterocladus antiquus* from the overlying Qinggouzi Formation (Zheng et al., 2023); a bipartite network analysis of microfossil assemblages indicates that the Qinggouzi Formation is best correlated with the early Tonian Gouhou Formation from the Huaibei Group (Zheng et al., 2023).

5.3. The carbon isotope record of the NCC

The new carbon isotope data from the Baishan strata were integrated with existing data from Pyongnam (Park et al., 2016), Dalian (Zhang et al., 2021), and Huaibei (Xiao et al., 2014) areas in the NCC for stratigraphic correlation using DTW (Figs. 2 and 6A). To initiate this process, we aligned and then merged the Pyongnam and Dalian data because both capture a ca. –5 ‰ excursion at the top of the section. The alignment with the highest cross-correlation value (0.93) was selected. This choice is supported by the alignment of radiometric dates within this framework and the absence of unrealistically large depositional gaps in the merged chemostratigraphic sequence (i.e., data points remained evenly distributed), given there is no evidence for large unconformities in the aligned sections. In the next step, the Huaibei sequence was correlated with and incorporated into the newly merged dataset containing the Pyongnam and Dalian data. Here again, we opted for the alignment with the highest cross-correlation value (0.82), following the same rationale as in the initial integration. As a result, the ∼5 ‰ decreasing trend at the uppermost portion of the Huaibei sequence was aligned with the descending limb of the negative excursion identified in the Pyongnam and Dalian sequences. Based on the in-situ U-Pb dating of early diagenetic microspar samples from the Weiji Formation (1010 ± 36 Ma) (Lan et al., 2022), this negative excursion likely occurred at ca. 1.0 Ga. Finally, the Baishan sequence was integrated into the dataset. The results show that this negative excursion is not captured in our data, which come from the upper Wanlong and lower Badaojiang formations. Instead, this negative excursion would likely postdate the lower Badaojiang Formation. Thus, the upper Badaojiang Formation should be a focus for future exploration of this excursion in the Jilin area to better constrain the correlation between the Baishan section and other sections in the NCC.

It is important to acknowledge that while we chose the alignment with the highest cross-correlation value (0.92) for this integration, uncertainties persist due to the dearth of radiometric dates and distinct isotopic features in the Baishan sequence. As this correlation predicts that the negative excursion would postdate the Wanlong Formation and the lower Badaojiang Formation, the upper Badaojiang Formation should be a focus for future exploration of this excursion in the Jilin area to better constrain the correlation between the Baishan section and other

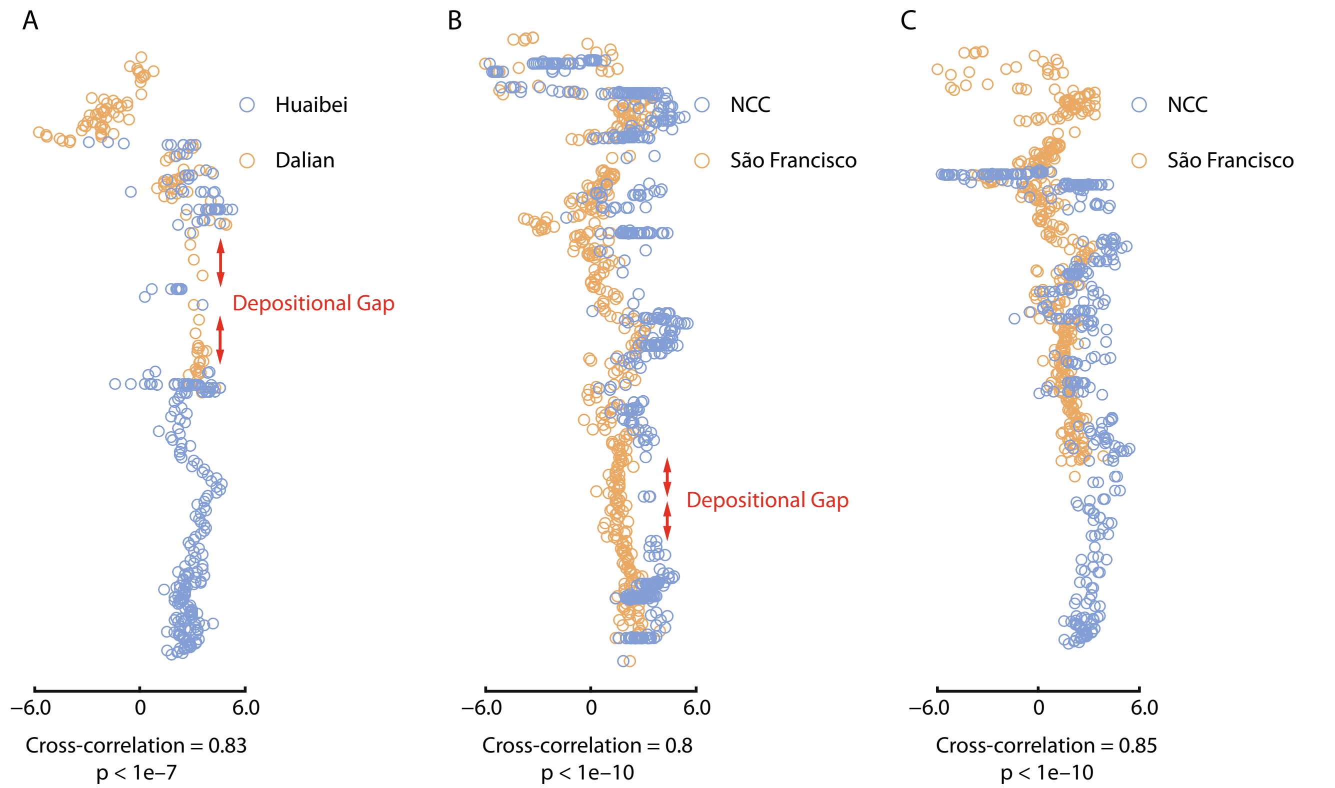

Fig. 7. Alternative alignments between the Huaibei and Dalian sequences (A) and between the assembled North China sequence and the São Francisco sequence (B and C). (A and B) These two alignments imply large depositional gaps in the Huaibei sequence and the assembled North China sequence. (C) This alignment fails to match the negative excursion in the two sequences. $\delta^{13}C_{carb}$ data are included in Data file S2.

sections in the NCC. Other orders of sequential correlation have also been tested but failed to produce meaningful alignments (see, for example, Fig. 7A for aligning the Dalian and Huaibei sequences first). This newly established, statistically significant integration unveils two distinct phases of the late Mesoproterozoic to early Neoproterozoic $\delta^{13}C_{carb}$ record in the NCC (Fig. 6): an interval marked by relatively moderate $\delta^{13}C$ variations with consistently positive values extending over approximately 50 million years, followed by a moderate negative excursion at the Mesoproterozoic and Neoproterozoic boundary (ca. 1 Ga).

5.4. A tentative global stratigraphic framework for the Meso-Neoproterozoic transition

To construct a global stratigraphic framework for the Meso-Neoproterozoic transition, we compared the newly integrated $\delta^{13}C_{carb}$ record of the NCC with $\delta^{13}C_{carb}$ data from the São Francisco and Congo cratons (Figs. 2 and 6B). Specifically, data from the Vazante Group (Alvarenga et al., 2019) deposited near the western border of the São Francisco Craton and the Mbuji-Mayi Supergroup (Delpomdor and Préat, 2013) deposited on the Congo Craton were used for this exercise. Both units have been assigned an late Mesoproterozoic to early Neoproterozoic age based on available radiometric dates, paleontological evidence, and carbon and strontium isotope data (Delpomdor et al., 2013a; Delpomdor and Préat, 2013; Baludikay et al., 2016; Alvarenga et al., 2019; Caxito et al., 2019; François et al., 2023). Previous research suggested a Neoproterozoic paleogeographic connection between the NCC and the São Francisco and Congo cratons on the basis of similar sediment provenance (Sun et al., 2020; Sun et al., 2022) and igneous dikes of similar lithology and ages (Peng et al., 2011; Cederberg et al., 2016; de Oliveira Chaves et al., 2019). However, paleomagnetic data present a different view, showing that the NCC and the São Francisco and Congo cratons were unlikely to have been paleogeographically connected during this interval (Zhao et al., 2020; Evans, 2021). Given that the paleomagnetic data provide more direct evidence of paleogeographic location, and that sediment provenance and magmatic data do not necessarily demand unique paleogeographic reconstructions, we argue that the compilation of $\delta^{13}C_{carb}$ data from these three cratons would likely give a global rather than local or regional picture of the late Mesoproterozoic to early Neoproterozoic chemostratigraphy.

In contrast to the relatively straightforward alignments within the NCC, the cross-basin comparison of data from the three cratons presents greater challenges due to the potential influence on the $\delta^{13}C_{carb}$ record by local or regional processes in different cratons. When conducting chemostratigraphic alignment between the NCC and the São Francisco Craton, data were first normalized (i.e., subtracting the mean from the raw data and then divided by the standard deviation) because the Vazante Group has consistently lower $\delta^{13}C$ values compared with that of the NCC. Normalization was necessary because the overall lower $\delta^{13}C$ values could be driven by local or regional processes during or after deposition. For instance, cross-shelf seawater $\delta^{13}C$ gradients, due to the influx of remineralized organic carbon from intertidal creeks, have been observed in the modern Great Bahama Bank (Geyman and Maloof, 2021). Additionally, the formation of authigenic carbonate during early diagenesis can decrease the $\delta^{13}C$ values of bulk samples (Schrag et al., 2013). Given the available radiometric dates, however, it is likely that the negative carbon isotope excursions recorded in both cratons may represent global signatures. To facilitate their correlation, we selected an alignment with a cross-correlation value of 0.74 (Fig. 6B), and while alignments with higher cross-correlation values were available, they either resulted in large depositional hiatuses that were not supported by sedimentary evidence (Fig. 7B) or failed to accurately match the excursions (Fig. 7C).

For the chemostratigraphic correlation between the NCC and the Congo Craton, we propose that the most negative $\delta^{13}C$ values within an up-section increasing trend in the lower Mbuji-Mayi Supergroup

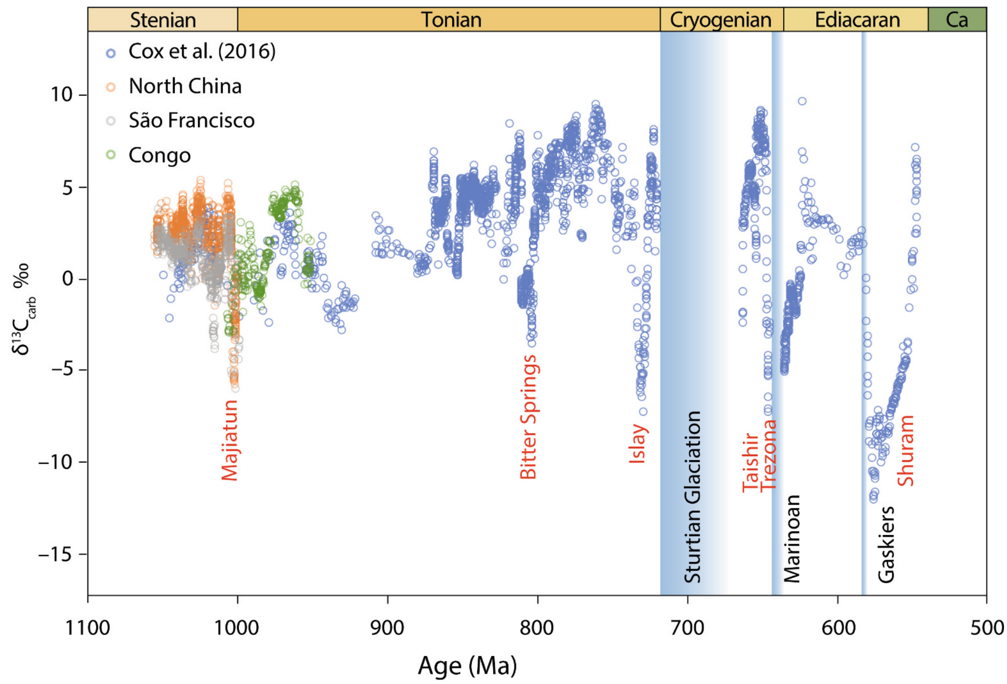

Fig. 8. Compilation of carbonate carbon isotope data for the Neoproterozoic Era. Modified after Cox et al. (2016). The ca. 1.0 Ga negative excursion (Majiatun excursion) identified in this study is likely the oldest negative excursion in the Neoproterozoic Era. $\delta^{13}C_{carb}$ data are included in Data files S1–S3.

(specifically, the BIIa – BIIc subgroups) capture the rising limb of the ca. 1.0 Ga negative excursion. Previous research suggested that the negative values within the BIIa – BIIc subgroups corresponded to the Bitter Springs Anomaly (Delpomdor and Préat, 2013). However, available radiometric dates indicate that the BIIa – BIIc subgroups are older than 1006 ± 13 Ma (François et al., 2023), thus predating the ca. 810 Ma Bitter Springs event (Macdonald et al., 2010; Cohen et al., 2017; Halverson et al., 2018). To accurately align the negative excursions, we used an edge value of 0.005, a selection driven by the limited overlap between the two $\delta^{13}C_{carb}$ profiles. Additionally, the cross-correlation value was not calculated for this alignment, because that the overlap between the records was less than 10 % (Fig. 6B).

By consolidating data from these three cratons, we have established a tentative chemostratigraphic framework for the Meso-Neoproterozoic transition (Figs. 2, 6, and 8). This framework reaffirms the moderate variability of the late Mesorpoterozoic $\delta^{13}C$ record, but also underscores the possibility that the ca. 1.0 Ga negative $\delta^{13}C_{carb}$ excursion, previously described as the Majiatun excursion from the Dalian region in the NCC (Zhang et al., 2021), could potentially be a global signal, given the presence of this excursion across multiple cratons. We note, however, that DTW can could force the correlation of local excursions as it is designed to mathematically align chemostratigraphic signals (Hagen and Creveling, 2024). Thus, while existing age constraints are consistent with our favored alignment, future investigations are needed to obtain higher-resolution radiometric dates across these three cratons to further confirm that this excursion is a globally synchronous event. If confirmed, the Majiatun excursion would represent a negative excursion right at the Meso-Neoproterozoic transition and marks the onset of Neoproterozoic carbon cycle volatility (Fig. 8). Given that the Majiatun excursion occurs at the Mesoproterozoic and Neoproterozoic boundary, it also holds the potential to serve as an important and useful marker of the beginning of the Neoproterozoic Era.

6. Conclusions

Available radiometric, paleontological, and chemostratigraphic data suggest that the Hunjiang Group at the Baishan area in North China is late Mesoproterozoic to early Neoproterozoic in age. Integrating new and existing $\delta^{13}C_{carb}$ chemostratigraphic data from the North China, São Francisco, and Congo cratons, we constructed a chemostratigraphic framework for the Meso-Neoproterozoic transition, using the dynamic time warping algorithm. The framework confirmed the moderate variability of the $\delta^{13}C_{carb}$ record in the late Mesoproterozoic and suggested the ca. 1.0 Ga Majiatun excursion as a potential global $\delta^{13}C_{carb}$ chemostratigraphic feature, which is a different event from the Bitter Springs Anomaly. This excursion likely marks the onset of the Neoproterozoic Era and the beginning of a more dynamic carbon cycle.

Supplementary data to this article can be found online at https://doi.org/10.1016/j.palaeo.2024.112505.

CRediT authorship contribution statement

Junyao Kang: Writing – original draft, Investigation, Formal analysis, Data curation, Conceptualization. **Qing Tang:** Writing – review & editing, Investigation. **Benjamin C. Gill:** Writing – review & editing, Investigation, Conceptualization. **Rachel Reid:** Writing – review & editing, Investigation. **Wentao Zheng:** Writing – review & editing, Investigation. **Shuhai Xiao:** Writing – original draft, Supervision, Project administration, Funding acquisition, Conceptualization.

Declaration of competing interest

The authors declare that they have no known competing financial interests or personal relationships that could have appeared to influence the work reported in this paper.

Data availability

Data are available in the main text or supplementary materials.

Acknowledgments

The research was supported by National Science Foundation (EAR-2021207), National Natural Science Foundation of China (42272001 to

Q.T.), and National Key Research and Development Program of China (2022YFF0800303 to Q.T.). We would like to thank Kai Xiang and Chengxi Wu for field assistance, Jeffrey Parks for technical assistance in geochemical analysis, and Cedric Hagen for help in dynamic time warping analysis.

References

Alvarenga, C.J., Oliveira, G.D., Vieira, L.C., Santos, R.V., Baptista, M.C., Dantas, E.L., 2019. Carbonate chemostratigraphy of the Vazante Group, Brazil: a probable Tonian age. Precambrian Res. 331, 105378.

American Public Health Association, American Water Works Association, Water Environment Federation, 1998. Standard Methods for the Examination of Water and Wastewater, 20th ed. APHA-AWWA-WEF, Washington, D.C.

Azmy, K., Kendall, B., Creaser, R.A., Heaman, L., de Oliveira, T.F., 2008. Global correlation of the Vazante Group, São Francisco Basin, Brazil: Re-Os and U-Pb radiometric age constraints. Precambrian Res. 164, 160–172.

Baludikay, B.K., Storme, J.-Y., François, C., Baudet, D., Javaux, E.J., 2016. A diverse and exquisitely preserved organic-walled microfossil assemblage from the Meso-Neoproterozoic Mbuji-Mayi Supergroup (Democratic Republic of Congo) and implications for Proterozoic biostratigraphy. Precambrian Res. 281, 166–184.

Bold, U., Ahm, A.-S.C., Schrag, D.P., Higgins, J.A., Jamsran, E., Macdonald, F.A., 2020. Effect of dolomitization on isotopic records from Neoproterozoic carbonates in southwestern Mongolia. Precambrian Res. 350, 105902.

Brand, U., Veizer, J., 1980. Chemical diagenesis of a multicomponent carbonate system; 1, Trace elements. J. Sediment. Res. 50, 1219–1236.

Brand, U., Veizer, J., 1981. Chemical diagenesis of a multicomponent carbonate system; 2, Stable isotopes. J. Sediment. Res. 51, 987–997.

Brocks, J.J., Jarrett, A.J.M., Sirantoine, E., Hallmann, C., Hoshino, Y., Liyanage, T., 2017. The rise of algae in Cryogenian oceans and the emergence of animals. Nature 548, 578–581.

Brocks, J.J., Nettersheim, B.J., Adam, P., Schaeffer, P., Jarrett, A.J., Güneli, N., Liyanage, T., van Maldegem, L.M., Hallmann, C., Hope, J.M., 2023. Lost world of complex life and the late rise of the eukaryotic crown. Nature 618, 767–773.

Bureau of Geology and Mineral Resources of Jilin Province, 1988. Regional Geology of Jilin Province. In: Chinese Ministry of Geology and Mineral Resources, Geological Memoirs, Series 1, Number 10. Geological Publishing House, Beijing.

Caxito, F.D.A., Uhlein, G.J., Uhlein, A., Pedrosa-Soares, A.C., Kuchenbecker, M., Reis, H., Sial, A.N., Ferreira, V.P., Alvarenga, C.J.S., Santos, R.V., 2019. Isotope stratigraphy of Precambrian sedimentary rocks from Brazil: Keys to unlock Earth's hydrosphere, biosphere, tectonic, and climate evolution, Stratigraphy & Timescales. Elsevier, pp. 73–132.

Cederberg, J., Söderlund, U., Oliveira, E.P., Ernst, R.E., Pisarevsky, S.A., 2016. U-Pb baddeleyite dating of the Proterozoic Pará de Minas dyke swarm in the São Francisco craton (Brazil)–implications for tectonic correlation with the Siberian, Congo and North China cratons. Gff 138, 219–240.

Cohen, P.A., Strauss, J.V., Rooney, A.D., Sharma, M., Tosca, N., 2017. Controlled hydroxyapatite biomineralization in an ~810 million-year-old unicellular eukaryote. Sci. Adv. 3, e1700095.

Cornet, Y., François, C., Compère, P., Callec, Y., Roberty, S., Plumier, J.C., Javaux, E.J., 2019. New insights on the paleobiology, biostratigraphy and paleogeography of the pre-Sturtian microfossil index taxon *Cerebrosphaera*. Precambrian Res. 332, 105410.

Cox, G.M., Halverson, G.P., Stevenson, R.K., Vokaty, M., Poirier, A., Kunzmann, M., Li, Z.-X., Denyszyn, S.W., Strauss, J.V., Macdonald, F.A., 2016. Continental flood basalt weathering as a trigger for Neoproterozoic Snowball Earth. Earth Planet. Sci. Lett. 446, 89–99.

de Oliveira Chaves, A., Ernst, R.E., Söderlund, U., Wang, X., Naeraa, T., 2019. The 920–900 Ma Bahia-Gangila LIP of the São Francisco and Congo cratons and link with Dashigou-Chulan LIP of North China craton: New insights from U-Pb geochronology and geochemistry. Precambrian Res. 329, 124–137.

Delpomdor, F., Préat, A., 2013. Early and late Neoproterozoic C, O and Sr isotope chemostratigraphy in the carbonates of West Congo and Mbuji-Mayi supergroups: a preserved marine signature? Palaeogeogr. Palaeoclimatol. Palaeoecol. 389, 35–47.

Delpomdor, F., Blanpied, C., Virgone, A., Préat, A., 2013a. Paleoenvironments in Meso–Neoproterozoic carbonates of the Mbuji-Mayi Supergroup (Democratic Republic of Congo)–Microfacies analysis combined with C–O–Sr isotopes, major-trace elements and REE+ Y distributions. J. Afr. Earth Sci. 88, 72–100.

Delpomdor, F., Linnemann, U., Boven, A., Gärtner, A., Travin, A., Blanpied, C., Virgone, A., Jelsma, H., Preat, A., 2013b. Depositional age, provenance, and tectonic and paleoclimatic settings of the late Mesoproterozoic–middle Neoproterozoic Mbuji-Mayi Supergroup, Democratic Republic of Congo. Palaeogeogr. Palaeoclimatol. Palaeoecol. 389, 4–34.

Dong, L., Xiao, S., Shen, B., Yuan, X., Yan, X., Peng, Y., 2008. Restudy of the worm-like carbonaceous compression fossils *Protoarenicola*, *Pararenicola*, and *Sinosabellidites* from early Neoproterozoic successions in North China. Palaeogeogr. Palaeoclimatol. Palaeoecol. 258, 138–161.

Evans, D.A., 2021. Meso-Neoproterozoic Rodinia supercycle, Ancient Supercontinents and the Paleogeography of Earth. Elsevier, pp. 549–576.

François, C., Baludikay, B., Debaille, V., Birck, J., Limmois, D., Jourdan, F., Baudet, D., Paquette, J., Delvaux, D., Javaux, E., 2023. Multi-method dating constrains the diversification of early eukaryotes in the Proterozoic Mbuji-Mayi Supergroup of the DR Congo and the geological evolution of the Congo Basin. J. Afr. Earth Sci. 198, 104785.

Fu, X., Zhang, S., Li, H., Ding, J., Li, H., Yang, T., Wu, H., Yuan, H., Lv, J., 2015. New paleomagnetic results from the Huaibei Group and Neoproterozoic mafic sills in the North China Craton and their paleogeographic implications. Precambrian Res. 269, 90–106.

Gao, L., Xing, Y., Liu, G., 1995. Neoproterozoic micropalaeoflora from Hunjiang area, Jilin Province and its sedimentary environment. Professional Papers of Stratigraphy and Palaeontology 26, 1–23.

Geyman, E.C., Maloof, A.C., 2019. A diurnal carbon engine explains ¹³C-enriched carbonates without increasing the global production of oxygen. Proc. Natl. Acad. Sci. 116, 24433–24439.

Geyman, E.C., Maloof, A.C., 2021. Facies control on carbonate $\delta^{13}C$ on the Great Bahama Bank. Geology 49, 1049–1054.

Guilbaud, R., Poulton, S.W., Butterfield, N.J., Zhu, M., Shields-Zhou, G.A., 2015. A global transition to ferruginous conditions in the early Neoproterozoic oceans. Nat. Geosci. 8, 466–470.

Hagen, C.J., Creveling, J.R., 2024. An algorithm-guided Ediacaran global composite δ13Ccarb–Bayesian age model. Palaeogeogr. Palaeoclimatol. Palaeoecol. 650, 112321.

Hagen, C.J., Harper, J.T., 2023. Dynamic time warping to quantify age distortion in firn cores impacted by melt processes. Ann. Glaciol. 1–9.

Hagen, C.J., Reilly, B.T., Stoner, J.S., Creveling, J.R., 2020. Dynamic time warping of palaeomagnetic secular variation data. Geophys. J. Int. 221, 706–721.

Hagen, C., Creveling, J., Huybers, P., 2024. Align: a user-friendly app for numerical stratigraphic correlation. GSA Today 34, 4–9.

Halverson, G.P., Hoffman, P.F., Schrag, D.P., Maloof, A.C., Rice, A.H.N., 2005. Toward a Neoproterozoic composite carbon-isotope record. GSA Bull. 117, 1181–1207 doi: 1110.1130/B25630.25631.

Halverson, G.P., Porter, S.M., Gibson, T.M., 2018. Dating the late Proterozoic stratigraphic record. Emerging Topics in Life Sciences 2, 137–147.

Hay, C.C., Creveling, J.R., Hagen, C.J., Maloof, A.C., Huybers, P., 2019. A library of early Cambrian chemostratigraphic correlations from a reproducible algorithm. Geology 47, 457–460.

He, T., Zhou, Y., Vermeesch, P., Rittner, M., Miao, L., Zhu, M., Carter, A., Strandmann, P. A.E.P.V., Shields, G.A., 2017. Measuring the 'Great Unconformity' on the North China Craton using new detrital zircon age data. Geol. Soc. Lond. Spec. Publ. 448, 145–159.

Higgins, J.A., Blättler, C.L., Lundstrom, E.A., Santiago-Ramos, D.P., Akhtar, A.A., Crüger Ahm, A.S., Bialik, O., Holmden, C., Bradbury, H., Murray, S.T., Swart, P.K., 2018. Mineralogy, early marine diagenesis, and the chemistry of shallow-water carbonate sediments. Geochim. Cosmochim. Acta 220, 512–534.

Hu, B., Zhai, M., Li, T., Li, Z., Peng, P., Guo, J., Kusky, T.M., 2012. Mesoproterozoic magmatic events in the eastern North China Craton and their tectonic implications: Geochronological evidence from detrital zircons in the Shandong Peninsula and North Korea. Gondwana Res. 22, 828–842.

Kang, J., Gill, B., Reid, R., Zhang, F., Xiao, S., 2023. Nitrate limitation in early Neoproterozoic oceans delayed the ecological rise of eukaryotes. Sci. Adv. 9, eade9647.

Kaufman, A.J., Knoll, A.H., 1995. Neoproterozoic variations in the C-isotope composition of sea water: Stratigraphic and biogeochemical implications. Precambrian Res. 73, 27–49.

Knoll, A.H., Walter, M.R., 1992. Latest Proterozoic stratigraphy and Earth history. Nature 356, 673–678.

Kriscautzky, A., Kah, L.C., Bartley, J.K., 2022. Molar-tooth structure as a window into the deposition and diagenesis of Precambrian carbonate. Annu. Rev. Earth Planet. Sci. 50, 205–230.

Kusky, T.M., Li, J., 2003. Paleoproterozoic tectonic evolution of the North China Craton. J. Asian Earth Sci. 22, 383–397.

Lan, Z., Roberts, N.M., Zhou, Y., Zhang, S., Li, Z., Zhao, T., 2022. Application of in situ U-Pb carbonate geochronology to Stenian-Tonian successions of North China. Precambrian Res. 370, 106551.

Lau, K.V., Hardisty, D.S., 2022. Modeling the impacts of diagenesis on carbonate paleoredox proxies. Geochim. Cosmochim. Acta 337, 123–139.

Li, D., Luo, G., Tang, Q., She, Z., Xiao, S., 2023. New record of the green algal fossil Proterocladus and coexisting microfossils from the Meso-Neoproterozoic Diaoyutai Formation in southern Liaoning, North China. Precambrian Res. 393, 107104.

Lisiecki, L.E., Lisiecki, P.A., 2002. Application of dynamic programming to the correlation of paleoclimate records. Paleoceanography 17, 1-1-1-12.

Macdonald, F.A., Schmitz, M.D., Crowley, J.L., Roots, C.F., Jones, D.S., Maloof, A.C., Strauss, J.V., Cohen, P.A., Johnston, D.T., Schrag, D.P., 2010. Calibrating the Cryogenian. Science 327, 1241–1243.

Meng, Q., Wei, H., Qu, Y., Ma, S., 2011. Stratigraphic and sedimentary records of the rift to drift evolution of the northern North China craton at the Paleo-to Mesoproterozoic transition. Gondwana Res. 20, 205–218.

Pang, K., Tang, Q., Wan, B., Yuan, X., 2020. New insights on the palaeobiology and biostratigraphy of the acritarch Trachyhystrichosphaera aimika: a potential late Mesoproterozoic to Tonian index fossil. Palaeoworld 29, 476–489.

Park, H., Zhai, M., Yang, J., Peng, P., Kim, J., Zhang, Y., Kim, M., Park, U., Feng, L., 2016. Deposition age of the Sangwon Supergroup in the Pyongnam basin (Korea) and the early Tonian negative carbon isotope interval. Acta Petrol. Sin. 32, 2181–2195.

Peng, P., Zhai, M., Li, Q., Wu, F., Hou, Q., Li, Z., Li, T., Zhang, Y., 2011. Neoproterozoic (~ 900 Ma) Sariwon sills in North Korea: Geochronology, geochemistry and implications for the evolution of the south-eastern margin of the North China Craton. Gondwana Res. 20, 243–254.

Qiao, X., Gao, L., Gao, L., Fu, G., Yin, C., Xie, X., Zhou, X., Chen, Y., 1995. Outcrop sequence stratigraphy of the Neoproterozoic in the Hunjiang Area, Jilin Province. Reginal Geology of China 2, 99–111.

Reinhard, C.T., Planavsky, N.J., Gill, B.C., Ozaki, K., Robbins, L.J., Lyons, T.W., Fischer, W.W., Wang, C., Cole, D.B., Konhauser, K.O., 2017. Evolution of the global phosphorus cycle. Nature 541, 386–389.

Rodrigues, J., Pimentel, M.M., Buhn, B., Matteini, M., Dardenne, M., Alvarenga, C., Armstrong, R., 2012. Provenance of the Vazante Group: New U-Pb, Sm-Nd, Lu-Hf isotopic data and implications for the tectonic evolution of the Neoproterozoic Brasília Belt. Gondwana Res. 21, 439–450.

Sakoe, H., Chiba, S., 1978. Dynamic programming algorithm optimization for spoken word recognition. IEEE Trans. Acoust. Speech Signal Process. 26, 43–49.

Schrag, D.P., Higgins, J.A., Macdonald, F.A., Johnston, D.T., 2013. Authigenic carbonate and the history of the global carbon cycle. Science 339, 540–543.

Su, X., Peng, P., Zhu, R., Mao, Y., Zhang, Z., Sun, F., 2020. Multi-stage evolution of the Xuhuai rift: Insights from the occurrence and compositional profiles of doleritic sills in the southeastern margin of the North China Craton. Gondwana Res. 82, 221–240.

Su, X., Peng, P., Foley, S., Teixeira, W., Zhai, M., 2021. Initiation of continental breakup documented in evolution of the magma plumbing system of the ca. 925 Ma Dashigou large igneous province, North China. Lithos 384, 105984.

Sun, F., Peng, P., Zhou, X., Magalhaes, A., Guadagnin, F., Zhou, X., Zhang, Z., Su, X., 2020. Provenance analysis of the late Mesoproterozoic to Neoproterozoic Xuhuai Basin in the southeast North China Craton: Implications for paleogeographic reconstruction. Precambrian Res. 337, 105554.

Sun, F., Peng, P., Zheng, D., Zuo, P., 2022. Reappraising the provenance of early Neoproterozoic strata in the southern–southeastern North China Craton and its implication for paleogeographic reconstruction. Minerals 12, 510.

Swart, P.K., 2015. The geochemistry of carbonate diagenesis: the past, present and future. Sedimentology 62, 1233–1304.

Tang, Q., Pang, K., Yuan, X., Wan, B., Xiao, S., 2015. Organic-walled microfossils from the Tonian Gouhou Formation, Huaibei region, North China Craton, and their biostratigraphic implications. Precambrian Res. 266, 296–318.

Tang, Q., Pang, K., Yuan, X., Xiao, S., 2020. A one-billion-year-old multicellular chlorophyte. Nature Ecology & Evolution 4, 543–549.

Trower, E.J., Hibner, B.M., Lincoln, T.A., Dodd, J.E., Hagen, C.J., Cantine, M.D., Gomes, M.L., 2024. Revisiting Elevated δ13C Values of Sediment on Modern Carbonate Platforms. Geophys. Res. Lett. 51 e2023GL107703.

Wen, Z., Fulai, L., Chaohui, L., 2020. Detrital zircon U-Pb ages of the late Mesoproterozoic–Neoproterozoic Qiaotou formation in the Liao-Ji area of the North China Craton: implications for Rodinia reconstruction. Int. Geol. Rev. 1–20.

Xiao, S., Tang, Q., 2018. After the boring billion and before the freezing millions: evolutionary patterns and innovations in the Tonian Period. Emerging Topics in Life Sciences 2, 161–171.

Xiao, S., Shen, B., Tang, Q., Kaufman, A.J., Yuan, X., Li, J., Qian, M., 2014. Biostratigraphic and chemostratigraphic constraints on the age of early Neoproterozoic carbonate successions in North China. Precambrian Res. 246, 208–225.

Xiao, S., Cui, H., Kang, J., McFadden, K.A., Kaufman, A.J., Kitajima, K., Fournelle, J.H., Schwid, M., Nolan, M., Baele, J.-M., Valley, J.W., 2020. Using SIMS to decode noisy stratigraphic δ13C variations in Ediacaran carbonates. Precambrian Res. 343, 105686.

Xu, J., Zhu, G., Tong, W., Cui, K., Liu, Q., 1987. Formation and evolution of the Tancheng-Lujiang wrench fault system: a major shear system to the northwest of the Pacific Ocean. Tectonophysics 134, 273–310.

Yang, D., Xu, W., Xu, Y., Wang, Q., Pei, F., Wang, F., 2012. U-Pb ages and Hf isotope data from detrital zircons in the Neoproterozoic sandstones of northern Jiangsu and southern Liaoning Provinces, China: implications for the Late Precambrian evolution of the southeastern North China Craton. Precambrian Res. 216, 162–176.

Yin, C., 1985. Micropaleoflora from the late Precambrian in Huainan region of Anhui Province and its stratigraphic significance. Professional Papers of Stratigraphy and Palaeontology, Chinese Academy of Geological Sciences 12, 97–119.

Yin, L., 1987. Microbiotas of latest Precambrian sequences in China. In: Nanjing Institute of Geology and Palaeontology Academica Sinica (Ed.), Stratigraphy and Palaeontology of Systemic Boundaries in China: Precambrian–Cambrian Boundary (1). Nanjing University Press, Nanjing, pp. 415–494.

Zhai, M., Hu, B., Zhao, T., Peng, P., Meng, Q., 2015. Late Paleoproterozoic–Neoproterozoic multi-rifting events in the North China Craton and their geological significance: a study advance and review. Tectonophysics 662, 153–166.

Zhang, S., Zhao, Y., Ye, H., Hu, G., 2016. Early Neoproterozoic emplacement of the diabase sill swarms in the Liaodong Peninsula and pre-magmatic uplift of the southeastern North China Craton. Precambrian Res. 272, 203–225.

Zhang, Z., Peng, P., Feng, L., Gong, Z., Mitchell, R.N., Li, Y., 2021. Oldest-known Neoproterozoic carbon isotope excursion: earlier onset of Neoproterozoic carbon cycle volatility. Gondwana Res. 94, 1–11.

Zhang, S., Cao, R., Lan, Z., Li, Z., Zhao, Z., Wan, B., Guan, C., Yuan, X., 2022. SIMS Pb-Pb dating of phosphates in the Proterozoic strata of SE North China Craton: Constraints on eukaryote evolution. Precambrian Res. 371, 106562.

Zhao, G., Sun, M., Wilde, S.A., Li, S., 2003. Assembly, accretion and breakup of the Paleo-Mesoproterozoic Columbia Supercontinent: records in the North China Craton. Gondwana Res. 6, 417–434.

Zhao, H., Zhang, S., Ding, J., Chang, L., Ren, Q., Li, H., Yang, T., Wu, H., 2020. New geochronologic and paleomagnetic results from early Neoproterozoic mafic sills and late Mesoproterozoic to early Neoproterozoic successions in the eastern North China Craton, and implications for the reconstruction of Rodinia. GSA Bull. 132, 739–766.

Zheng, W., Tang, Q., Xiao, S., Pang, K., Kang, J., Li, G., Zhou, C., Yuan, X., Wan, B., 2023. The Proterozoic Qinggouzi microfossil assemblage and its biostratigraphic constraints on the Great Unconformity in northeastern North China Craton. Precambrian Res. 395, 107130.

Zhu, G., Wang, Y., Liu, G., Niu, M., Xie, C., Li, C., 2005. 40Ar/39Ar dating of strike-slip motion on the Tan–Lu fault zone, East China. J. Struct. Geol. 27, 1379–1398.

Zhu, R., Ni, P., Wang, G., Ding, J., Fan, M., Ma, Y., 2019. Geochronology, geochemistry and petrogenesis of the Laozhaishan dolerite sills in the southeastern margin of the North China Craton and their geological implication. Gondwana Res. 67, 131–146.

Zumberge, J.A., Rocher, D., Love, G.D., 2020. Free and kerogen-bound biomarkers from late Tonian sedimentary rocks record abundant eukaryotes in mid-Neoproterozoic marine communities. Geobiology 18, 326–347.